Chinese Journal of Aeronautics, (2020), xxx(xx): xxx–xxx

Chinese Society of Aeronautics and Astronautics
& Beihang University

**Chinese Journal of Aeronautics**

cja@buaa.edu.cn
www.sciencedirect.com

# Simulation of temperature distribution and discharge crater of $SiC_p/Al$ composites in a single-pulsed arc discharge

**Jipeng CHEN [a,c], Lin GU [b,*], Wansheng ZHAO [b], Mario GUAGLIANO [c]**

[a] *School of Mechanical and Electronic Engineering, Nanjing Forestry University, Nanjing 210037, China*
[b] *State Key Laboratory of Mechanical System and Vibration, School of Mechanical Engineering, Shanghai Jiao Tong University, Shanghai 200240, China*
[c] *Department of Mechanical Engineering, Politecnico Di Milano, Piazza Leonardo da Vinci, 32, Italy*

Received 26 February 2020; revised 31 May 2020; accepted 31 May 2020

**KEYWORDS**

Arc discharge;
Discharge crater;
$SiC_p/Al$ composites;
Single-pulsed;
Temperature distribution

**Abstract** $SiC_p/Al$ composites are difficult-to-cut materials. In recent years, electrical arc discharge machining has been developed to improve the machinability of these materials. However, there is a big challenge to build a satisfactory heat transfer model of $SiC_p/Al$ composites in the arc machining. This is not only because of the material property difference between the reinforcement and matrix material but also because of the micro-dimension SiC reinforcements. This paper established a new heat conduction simulation model considering the SiC particle-Al matrix interface and the phase change effects in a single-pulsed arc discharge of $SiC_p/Al$ composites. A novel SiC particle-Al matrix cell geometric model was designed firstly. Then, the temperature distribution at a different depth from the workpiece surface was analyzed, the influence of sic volume fraction on temperature field was studied, and the contribution of the interface thermal resistance and latent heat were explained. To demonstrate the validity of the new numerical model, comparisons and verifications were employed. Finally, the method of improving the model was proposed and the machining mechanism of arc discharge of $SiC_p/Al$ matrix materials was discussed. It was found that high temperature is prone to concentrate on the surface layers of the workpiece especially when the SiC fraction is high, also, the temperature fluctuates respectively at the evaporation point of aluminum and SiC, and the SiC-Al resistance has less influence on temperature distribution compared to latent heat, etc. The model build in this work improves the simulation accuracy observably compared



* Corresponding author.
E-mail address: lgu@sjtu.edu.cn (L. GU).
Peer review under responsibility of Editorial Committee of CJA.

ELSEVIER Production and hosting by Elsevier

https://doi.org/10.1016/j.cja.2020.05.033


Please cite this article in press as: CHEN J et al. Simulation of temperature distribution and discharge crater of $SiC_p/Al$ composites in a single-pulsed arc discharge, *Chin J Aeronaut* (2020), https://doi.org/10.1016/j.cja.2020.05.033

to the previous model, and the simulation work will help to acquire a detailed mechanism of material removal of $SiC_p$/Al composites in the arc discharge machining.



## 1. Introduction

$SiC_p$/Al composites have high specific strength, specific stiffness and wear resistance, low thermal expansion coefficient, good fatigue resistance, thermal conductivity, and electrical conductivity. They have attracted much attention in the military, aerospace, and automotive industry, besides the electronic packaging and optics.[1–3] It is known that $SiC_p$/Al composites consist of reinforcement particles (SiC) and matrix material (aluminum alloys). Although the $SiC_p$/Al composites possess numerous excellent physical and mechanical properties, its natural characteristics of SiC particle's high hardness and high wear resistance lead to low tool life and poor machined surface quality, especially in machining aluminum matrix composites (AMCs) reinforced with a high fraction of SiC particulate.[4–7] Besides traditional cutting processes, e.g., turning, [8,9] milling, [5,10,11] drilling,[3,12] grinding,[4,13] non-traditional processes have also been adopted to machine $SiC_p$/Al. Among them, the Electric discharge machining (EDM) process[14–17] is widely employed. EDM process is a material removal process that relies on heat generation to melt and vaporize a select portion of the workpiece material by ionization within the dielectric medium, in which the workpiece is dipped.[18] One of the deficiencies of the EDM process lies in its limited machining efficiency. In EDM, the discharges between the electrode and workpiece are generally electrical sparks. Compared to spark discharges, electrical arc discharge has a lager discharge energy because a higher peak current and a longer pulse duration are generally employed. Hence, arc discharge machining processes, such as arc dimensional machining (ADM),[19] short electric arc machining,[20,21] combined machining of electrical discharge machining and arc machining,[22,23] electro-arc machining[24] have been proposed to improve the material removal ability of EDM.

Blasting erosion arc machining (BEAM) is also a typical applicable arc discharge process which was developed by Zhao and Gu around 2012.[25] BEAM has been used to machining difficult-to-cut materials such as titanium alloys,[26] nickel-based alloys[27] and demonstrated a very high material removal rate (MRR). Since 2014, Gu and Chen[28–30] conducted experiments on the machining of $SiC_p$/Al composites with BEAM and studied relevant processing properties. It was found that the MRR of machining 20vol% and 50vol% $SiC_p$/Al composites could be as high as 10,000 $mm^3$/min, and 7500 $mm^3$/min respectively. At present, research about heat transfer simulation of discharge machining $SiC_p$/Al composites has been conducted, for example, Gu et al.[31] built a heat transfer model to explain the heat affect zone (HAZ) of arc machining $SiC_p$/Al composites, Tang et al.[17] established an EDM continuous multi-pulse discharge temperature simulation model to explore characteristics of EDM of $SiC_p$/Al composite materials. However, the $SiC_p$/Al composites in the reported models are generally simplified as an isotropic homogeneous material, SiC particle-Al matrix interface effect, and phase change are normally not considered. It is predicted that the interfaces in composites materials seriously affect the thermal properties of the composites.[32] The interfacial thermal resistance reduces the conductivity of the composites, and this reduction can be very pronounced for small reinforcement particles.[33]

There is a big challenge to build a heat transfer model of $SiC_p$/Al l composites in the arc machining not only because of the material property difference but also because of the micro-dimension SiC reinforcement (e.g., 10 μm) which makes the geometry model very difficult. This paper attempts to establish a heat conduction simulation model with the consideration of the SiC particle-Al matrix interface and phase change effects during the single arc discharge. The simulation model will be verified and compared, the influence of SiC volume fraction and discharge energy on temperature field and crater dimension will also be researched. The simulation work will help to acquire a detailed mechanism of material removal of $SiC_p$/Al composites in arc discharge machining.

## 2. Simulation approach

### 2.1. Single arc discharge process

The schematic of a single pulse arc discharge is shown in Fig. 1. The copper electrode is fixed on the spindle of a CNC machine. The electrode moves with the spindle without rotating. The workpiece immerses in the dielectric (deionized water). The dielectric breaks down and an arc forms when the distance of the electrode and the workpiece is within the discharge gap. The power works in single discharge mode, hence there is one pulsed arc generates and forms one crater on the workpiece surface.

The occurrence of arc discharge and its heat conduction to $SiC_p$/Al composite workpiece is very complex, hence, necessary simplifications are employed.

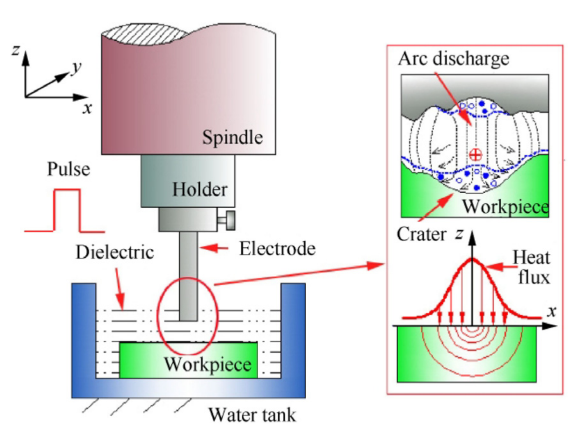


**Fig. 1** Schematic of a single-pulsed arc discharge.

(1) Neglecting the influence of the external environment on the arc plasma discharge. Assuming the energy of the arc discharge plasma assigned to the workpiece is constant.
(2) Neglecting the effect of working fluid on the heat transfer process of workpieces. Assuming that the phase changed material is removed from the workpiece and forms craters on the workpiece.
(3) Assuming the reinforcement particles are sphere-shape and uniformly distributed in the matrix material.
(4) Neglecting the chemical reactions between SiC reinforcement and Al matrix material (e.g., the occurrence of $Al_4C_3$) and not consider their influence on temperature.
(5) The computational domain is axisymmetrical and can be modeled in a two-dimensional coordinate.[34]

### 2.2. Numerical model

In this study, the construction of the numerical model is based on COMSOL Multiphysics 5.4. The Fouriers law of heat conduction and heat balance equation in solid is expressed as

$$\mathbf{q} = -k\nabla T \tag{1}$$

$$\rho C_p(\partial T/\partial t + u\nabla T) + \nabla \cdot \mathbf{q} = -\alpha T : dS/dt + \mathbf{q} \tag{2}$$

where $k$ is the thermal conductivity (W/(m·K)), $\rho$ is the density (kg/m$^3$), $C_p$ is the specific heat capacity at constant pressure (J/(kg·K)), $\boldsymbol{u}$ is the velocity vector (m/s), $\boldsymbol{q}$ is the heat flux by conduction (W/m$^2$), $\alpha$ is the coefficient of thermal expansion (1/K), $\boldsymbol{S}$ is the second Piola-Kirchhoff stress tensor (Pa), $Q$ is additional heat sources (W/m$^3$), $T$ is temperature.

To build a heat conduction model considering the interfacial effects of reinforcement particles and matrix material, a geometrical model containing both particle domain and matrix domain should be employed. However, the construction of the geometrical model will be very complex if a real-scale particle dimension is adopted, this is because the size of a SiC particle can be as small as 10 μm. Consequently, a compromised method is adopted. A square cell which contains SiC particle domain and the matrix domain is proposed, as shown in Fig. 2.

The length of the square cell ($L_{ce}$) is set as a constant, and $L_{ce}$ = 0.1 mm in this study. The radius of the particle is written as

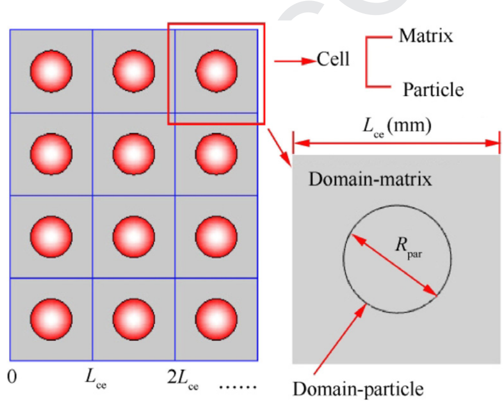


**Fig. 2** Construction of geometric model.

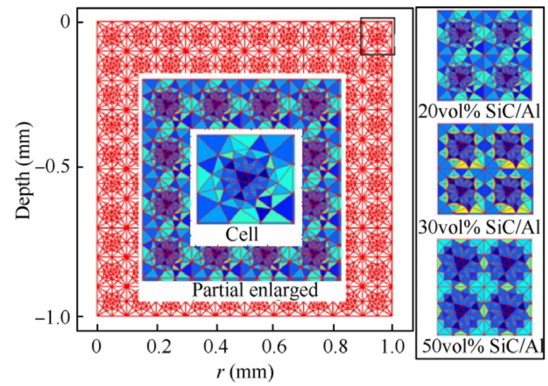


**Fig. 3** Full length geometric model with meshes.

$$R_{par} = \sqrt{\frac{f_{vol}{L_{ce}}^2}{\pi}} \tag{3}$$

where $f_{vol}$ is the volume fraction of SiC particles. With this method, the radiuses of SiC particles are 25.2 μm and 39.8 μm respectively when SiC volume fractions are 20% and 50%. Note that if the radiuses of SiC particles in the model are too small, the calculation will be very difficult and time-consuming, even not convergence. A full-length geometric model (two-dimensional axis-symmetry) with meshes (mesh size is chosen as "extra coarse") is shown in Fig. 3.

On most occasions, essential thermal properties of SiC are taken as constant. In this study, the temperature- dependent properties of SiC are taken into account, which is given by[35]

$$C_p(T) = 0.48 + 0.023\exp\left(\frac{T}{262}\right) \tag{4}$$

$$\lambda(T) = 2.67 \times 10^5 T^{-1.26} \tag{5}$$

where $C_p(T)$ is specific heat capacity function of temperature, $\lambda(T)$ is thermal conductivity function of temperature.

It is known that the aluminum solid changes to liquid/gas at the temperature of 933 K/2743 K, the corresponding latent heats are 390 kJ/kg and 11,834 kJ/kg respectively. The thermal properties of the liquid and gas states are expressed as a piecewise function of temperature. Here we use the piecewise functions that have been built in the COMSOL material database. Different from aluminum, it is generally regarded that SiC decomposes (SiC → Si + C) and evaporates at a temperature of 3100 K. Sometimes, a melting process is also observed, for example, a cloud of ejected liquid SiC material right above the target surface starts being observable from 1000 ns in a laser machining process.[36] Reference 37–39 explained that SiC becomes a solution of carbon in liquid silicon above melting temperature, and the thermal parameters of liquid SiC are represented by those of liquid silicon. In some study cases, the melting or evaporation of SiC is generally not considered.[40] In this study, we consider the evaporation of SiC but neglect its melting process since the pulse duration adopted in this research is less than 2 ms. The latent heat of SiC evaporation is 530 kJ/mol,[37,38] and the molecular weight of SiC is 40 g/mol,[41] so we take a value of 1.325 × 10$^4$ kJ/kg as the latent heat of SiC evaporation in the calculation. Furthermore, we take aluminum as matrix material and consider both the melting and evaporation of aluminum. We set the thermal



Please cite this article in press as: CHEN J et al. Simulation of temperature distribution and discharge crater of SiC$_p$/Al composites in a single-pulsed arc discharge, *Chin J Aeronaut* (2020), https://doi.org/10.1016/j.cja.2020.05.033

parameters of aluminum as constants in the solid phase (< 933 K). While in the liquid phase, the thermal conductivity is $33.9 + 0.07892\,T\text{-}2.099 \times 10^{-5}T^2$ W/(m·K) (933–1491 K) and 105 W/(m·K) (> 1491 K), and the specific heat is 1127 J/(kg·K) as reported in reference.[42]

In terms of interfacial resistance between SiC and Al, a value of $5.38 \times 10^{-9}$ K·m$^2$/W for 20 vol.% $SiC_p$/Al and value of $8.37 \times 10^{-9}$ K·m$^2$/W for 40vol% $SiC_p$/Al are reported.[33,43] The interfacial thermal resistance value for 20vol% $SiC_p$/Al is a little lower than that for 40vol% $SiC_p$/Al, which is also due to the dislocations induced by SiC-particle loading.[33] In this study, we use a linear fitting function to describe the interfacial resistance of different volume fraction $SiC_p$/Al composites based on the above two values. The thermal parameters of Al, SiC, and Al-SiC interface are also listed in Tables 1–3.

A Gaussian distribution heat flux $q(r)$ is employed as a heat source,[31,44,45] which is expressed as

$$\mathbf{q}(r) = \frac{3}{1-\exp(-3)} \cdot \frac{fUI}{\pi r_{\mathrm{P}}^2} . \exp\left[-3\left(\frac{r}{r_{\mathrm{p}}}\right)^2\right] \tag{6}$$

where $r$ is the distance from the center of the plasma column, $f$ is energy distribution coefficient and a value of 0.39 is generally adopted,[31,44,45] $U$ is discharge voltage which is generally a constant during discharge, $U$ = 25 V. $I$ is discharge current which can be taken as peak current value. Where $r_{\mathrm{p}}$ is the radius of the plasma heating area, generally, empirical formulas with discharge current and pulse on time ($t_{\mathrm{on}}$) are used to describe this parameter, e.g., $2.04 \times 10^{-3} I^{0.43} t_{\mathrm{on}}^{0.44}$,[17] $0.788 t_{\mathrm{on}}^{3/4}$.[44,46] Currently, there is no available radius of the plasma heating area function in the arc discharge machining, a constant value of 0.55 mm is adopted in this study based on previous measurement.[31] Note that this value is only for $SiC_p$/Al material under a low energy arc discharge condition. In our previous work, it has been demonstrated that discharge energy has a great influence on the material removal rate and HAZ.[28–31] Generally, higher energy means a larger material removal rate and a deeper HAZ. Since this study is focused on the interfacial resistant effects, the discharge parameters are selected as constant. A typical low energy arc discharge parameter combination and SiC fractions are shown in Table 4.

**Table 1** Thermal properties of Al.

| Quantity | Value |
| --- | --- |
| Density (kg/m$^3$) | 2700 |
| Specific heat (solid) (J/(kg·K)) | 900 |
| Thermal conductivity (solid) (W/(m·K)) | 238 |
| Melt point temperature (K) | 933 |
| Latent heat of melting (kJ/kg) | 390 |
| Evaporation point temperature (K) | 2743 |
| Latent heat of evaporation (kJ/kg) | 11,834 |
| Specific heat (liquid) (J/(kg·K)) | 1127 |
| Thermal conductivity (liquid < 1491 K) (W/(m·K)) | $33.9 + 0.07892\,T\text{-}2.099 \times 10^{-5}T^2$ |
| Thermal conductivity (liquid > 1491 K) (W/(m·K)) | 105 |

**Table 2** Thermal properties of SiC.

| Quantity | Value |
| --- | --- |
| Density (kg/m$^3$) | 3240 |
| Decomposition temperature (K) | 3100 |
| Specific heat (J/(kg·K)) | $0.48 + 0.023\exp(T/262)$ |
| Thermal conductivity (W/(m·K)) | $2.67 \times 10^5 T^{-1.26}$ |
| Latent heat of evaporation (kJ/kg) | $1.325 \times 10^4$ (530 kJ/mol) |

**Table 3** Al-SiC interfacial thermal property.

| Quantity | Value |
| --- | --- |
| Thermal resistance (K·myy$^2$/W) | $(14.95 f_{\mathrm{vol}} + 2.39) \times 10^{-9}$ |

**Table 4** Study parameters employed in simulations.

| Item | Parameters |
| --- | --- |
| Discharge voltage $U$ (V) | 25 |
| Discharge current $I$ (A) | 100 |
| Pulse on time $t_{\mathrm{on}}$ (ms) | 0–2.0 |
| SiC volume fraction $f_{\mathrm{vol}}$ (vol%) | 20, 30, 40, 50 |

## 3. Results, comparison and verification

### 3.1. Results

Fig. 4 shows a simulative 3D temperature calculation result of single-pulsed arc discharge of $SiC_p$/Al composites (20vol% and 50vol% $SiC_p$/Al), detailed temperature distributions are shown in Fig. 5 (20vol%, 30vol%, 40vol% and 50vol% $SiC_p$/Al). When the pulse on time reaches 2 ms, the peak surface temperature of $SiC_p$/Al workpiece is generally higher than 3300 K. At this temperature, the evaporations of both matrix material and SiC particles will happen. Also, the high temperature is found to concentrate on the surface layers of the workpiece, especially when the sic fraction is higher, it indicates that the SiC particles have a strong thermal resistant characteristic which is not conducive to thermal machining. There is another trend that the peak value of workpiece surface decreases with the increasing SiC fraction, which indicates that the SiC tends to absorb more heat energy and leads to a decline of temperature. The detailed mechanism has been discussed in reference.[31]

A detailed temperature increasing process at different depth ($r$ = 0.1 mm) is shown in Fig. 6. The workpiece with different SiC fractions appears a similar temperature increasing tendency. Once the heat source acts on the workpiece, the temperature increases quickly to the evaporation point of aluminum within 0.25 ms at the surface layers. Then, the temperature rises slowly. At the evaporation point of aluminum and SiC, the temperature fluctuation can be found respectively because of the high latent heat of aluminum (11,834 kJ/kg) and SiC

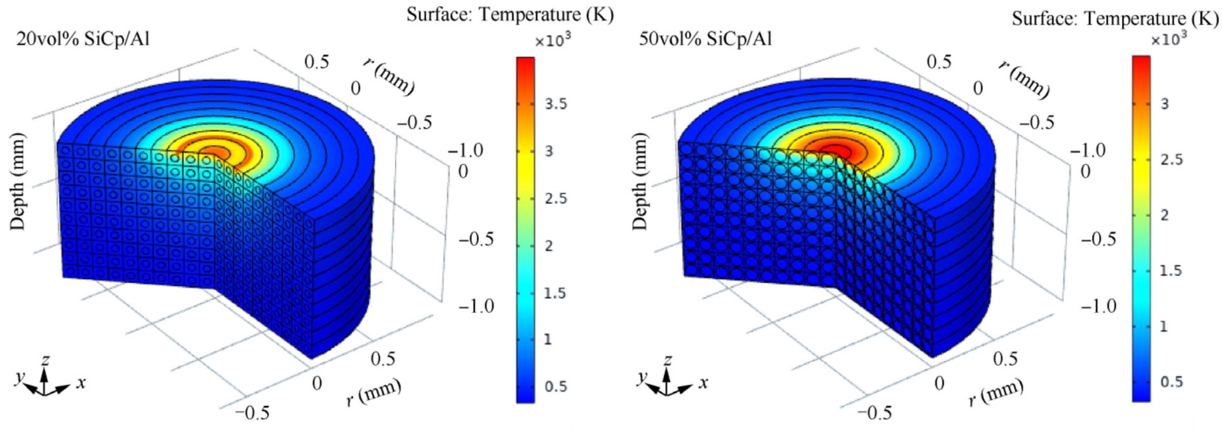


**Fig. 4** Simulative 3D temperature calculation result ($t_{on}$ = 2 ms).

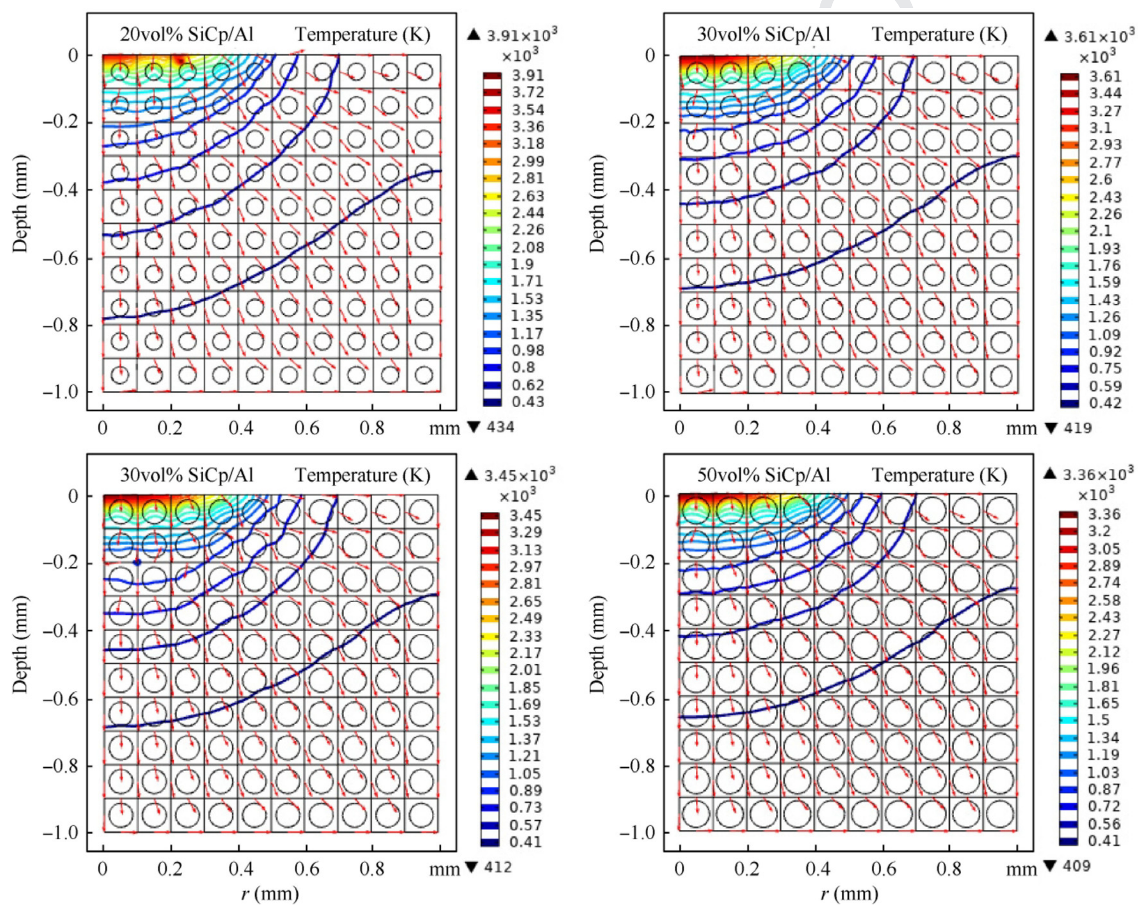


**Fig. 5** Temperature distribution in $SiC_p$/Al composites ($t_{on}$ = 2 ms).

(13,250 kJ/kg). Compared to latent heat, the SiC-matrix interface resistance has less influence on temperature distribution. At the depth of −0.1 mm, the temperatures of different SiC fraction workpiece increases over aluminum melting point within 5 ms respectively, and then slowly increases with time. The overall temperature is much lower than that of the surface layers. At this depth, the main phase change is the melting of the matrix material. At the depth of −0.2 mm, the material temperature is around the melting point of aluminum after 1.25 ms. Based on the temperature distribution observation, two mechanisms in the temperature increasing process can be known, i.e., the evaporation of SiC and aluminum, and the melting of aluminum. The former occurs on the surface of the workpiece, the later exits in the material interior.

### 3.2. Comparison and verification

In previous work, an equivalent heat conduction model (Gu's model) was built to demonstrate the influence of Sic particle on

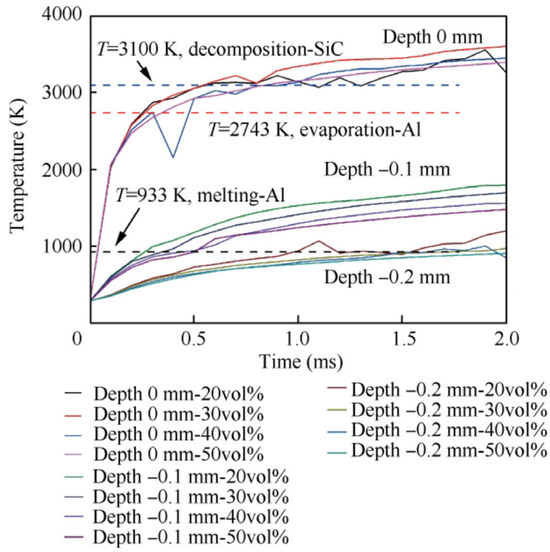


**Fig. 6** Temperature increasing process at different depth ($r$ = 0.1 mm).

the arc machining.[31] However, the workpiece materials are considered as homogeneous in Gu's model, and the thermal properties of the workpiece were calculated according to a combination of Al and SiC considering reinforcement fractions. To verify the advantage of the simulation model built in this work, the comparisons between the Gu's model and experiment results are conducted. The experimental setup was based on a needle-plane single arc discharge device. The workpiece materials used for single discharge experiments were 20vol% $SiC_p$/Al and 50vol% $SiC_p$/Al composites respectively. The experimental setup, results, and the discharge cater observations (with a laser confocal microscopy-ZEISS LSM700, as shown in Fig. 7) are available in reference.[31]

A comparison of a single discharge crater in Gu's model and this work is shown in Fig. 8. The crater in this work is smaller than that of Gu's model under the same discharge parameters. The surface of the discharge crater is also not as smooth as that of Gu's model, this phoneme demonstrates that the SiC particles tend to cause uneven microscopic surfaces (i.e., burr and flashing) which can be observed in Fig. 7. Both Gu's model and this work are compared with experimental results, as shown in Fig. 9. The maximum crater radiuses of the two models are close to the experimental values, this is because the plasma heating area value adopted in the models is based on the measurement, i.e. a constant value 0.55. However, the crater depths of Gu's model are much larger than the experimental values. Table 5 shows the error comparison with Gu's model. The errors of 20vol% $SiC_p$/Al and 50vol% $SiC_p$/Al crater depths can be as high as 54.5% and 68.7%, which indicates that the previous model method is far from satisfactory. In this work, a new modeling method is adopted, and the errors of crater depth can be reduced to 21.9% and 14.5% respectively, which improves the simulation precision greatly. It is noted that the reason why the new model not showing good enough characteristics for the radius of the discharge crater is that the actual radius of the plasma heating area is not the same for the different $SiC_p$/Al composites with different SiC fractions according to measurement value, however, this model uses a uniform value for simplification. Thus, compared to the discharge crater, the crater depth is paid more attention.

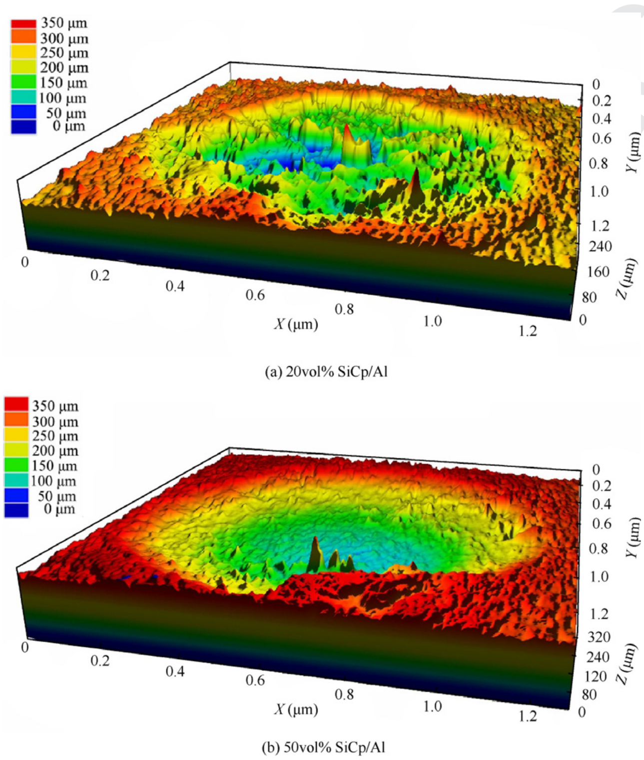


**Fig. 7** Single pulsed arc discharge crater measured with a laser confocal microscopy.[30,31]

## 4. Discussion

Many factors affect the precision of the simulation model. In this study, an energy distribution value of 0.39 is adopted. This energy distribution coefficient is widely used in traditional EDM studies.[44,45,47–49] However, in the arc discharge, the energy distribution coefficient is likely lower than this value, because the discharge gap in an arc discharge can be higher than 0.2 mm, which is larger than the EDM discharge gap. Thus, the arc plasma is easier to be involved in the heat exchange with the surrounding dielectric and leads to an extra energy loss. A correction coefficient can be employed to overcome this problem since the precise value of arc discharge distribution is not available currently. Table 6 shows the error values when adopting different correction coefficients. When the coefficients change from 1 to 0.8, the average error reduces and then increases. Considering a balance combination of discharge crater radius and depth, the coefficient value 0.85 is recommended in the simulation of arc discharge machining of $SiC_p$/Al composites.

Gu et al.[28,31] and Chen et al.[29] studied the processing and mechanism of machining $SiC_p$/Al composites, and it was found that SiC reinforcement has a negative influence on the machining efficiency, and HAZ thickness, etc. In term of the different discharge crater dimensions, it has been revealed that the extreme temperature-dependent prosperities of SiC reinforcement is the main reason. As shown in Fig. 10, the reinforcements tend to absorb more energy when the

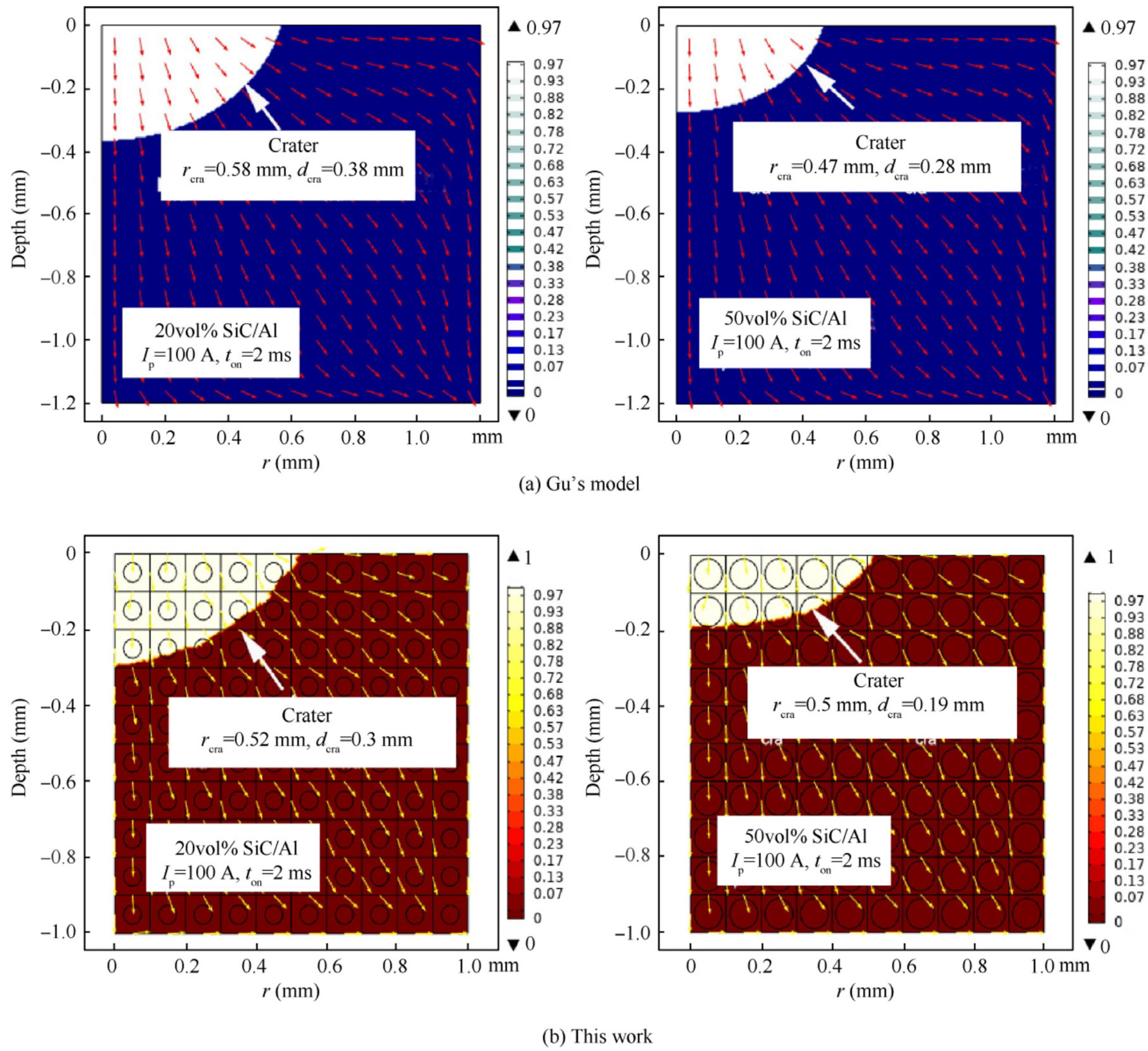


**Fig. 8** Comparison of single-pulsed arc discharge crater of $SiC_p$/Al composites.

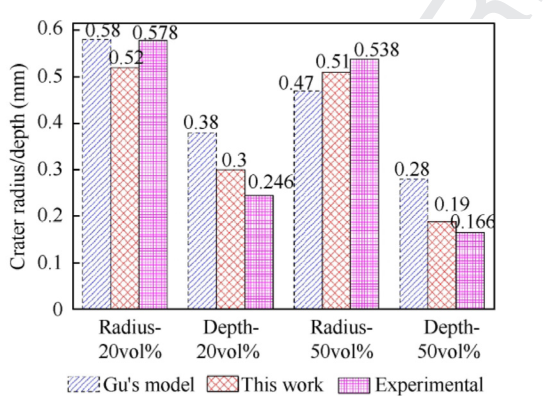


**Fig. 9** Comparison with Gu's model and experimental results.

temperature increases, as a result, higher reinforcement fraction will lead to a smaller discharge crater and lower machining efficiency. The viewpoint can be proved with the temperature distribution. For instance, the surface temperature of 20vol% $SiC_p$/Al material can be 550 K higher than that of 50vol% $SiC_p$/Al material. It is found that the higher temperature concentrates on the surface layers of the workpiece, especially when the sic fraction is higher. Since the heat is not easy to conduct and dissipate, the higher SiC fraction workpiece will have a thicker HAZ. For example, the HAZ thickness of 50vol% $SiC_p$/Al composites can be 2 times higher than that of 20vol% $SiC_p$/Al composites.[31]

Fig. 11 shows that the debris size and shape of blasting erosion arc machining $SiC_p$/Al materials are quite different. The low SiC fraction $SiC_p$/Al material debris has a larger size and contains full SiC particles inside, while most of the high SiC fraction $SiC_p$/Al material has a smaller size and even without containing SiC particle interiorly. Gu et al.[31] explained the above phenomenon with a hypothesis: a molten pool is filled with liquidated aluminum and solid SiC particles, the flowability of the molten aluminum with higher SiC fraction is much worse than that of the lower SiC fraction $SiC_p$/Al composites. Because the solid SiC particles are too much for the molten aluminum to take away, they tend to be left on the workpiece surface and sublimated by the arc plasma.

The temperature distribution observed in this work can be used to support Gu et al.'s hypothesis. The temperature of the

**Table 5** Error comparison with Gu's model.

| Model | Radius | | Depth | |
|---|---|---|---|---|
| | 20vol% | 50vol% | 20vol% | 50vol% |
| Gu's model | 0.3 % | 12.6 % | 54.5 % | 68.7 % |
| This work | 10 % | 5.2 % | ☆21.9 % | ☆14.5% |

**Table 6** Crater errors using different correction coefficients.

| Coefficient | Radius | | Depth | | Average |
|---|---|---|---|---|---|
| | 20vol% | 50vol% | 20vol% | 50vol% | |
| 1 | 10 % | 5.2 % | 21.9 % | 14.5 % | 12.9 % |
| 0.9 | 13.5 % | 7.0 % | 5.7 % | 11.4 % | 9.4 % |
| 0.85 | 15.2 % | 8.9 % | 1.6 % | 8.4 % | 8.5 % |
| 0.8 | 15.2% | 10.8 % | 6.5 % | 2.4 % | 8.7 % |

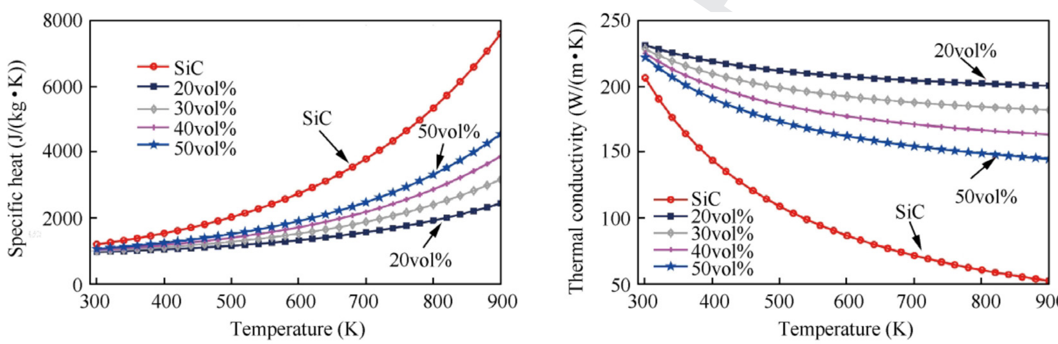


**Fig. 10** Equivalent thermal parameters of $SiC_p$/Al composites.

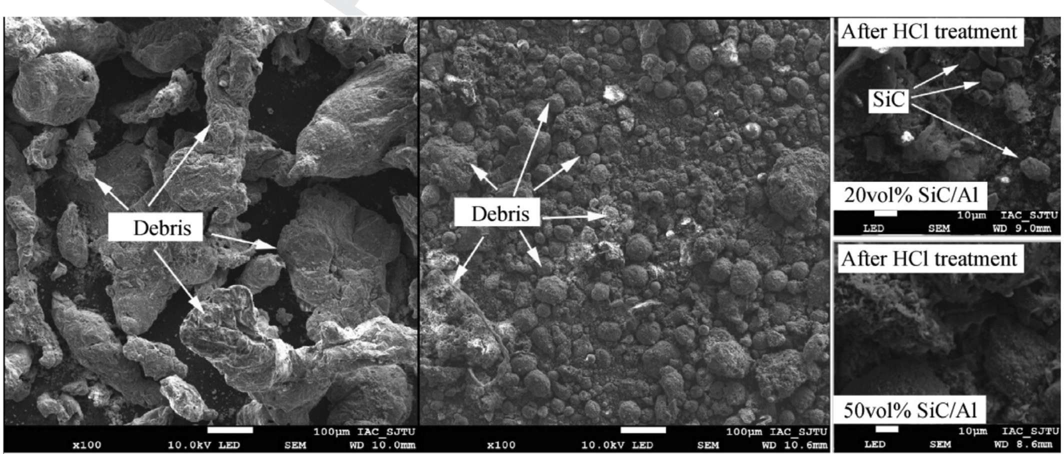


**Fig. 11** Discharge debris of $SiC_p$/Al composites.

workpiece surface layer is higher than the evaporation point of both Al and SiC, which will cause the sublimation of SiC and evaporation of Al. And the temperature is lower than 2743 K (evaporation point of Al) at a depth range from −0.1 mm to −0.3 mm, which will form a molten aluminum pool. Since the temperature increasing tendency is almost the same regardless of the SiC fractions, the melting and evaporation of different $SiC_p$/Al composites should be similar. The difference lies in the ejection process of the melton material. Since high SiC fraction material contains more SiC particles, they are overheated by plasmas without the full protection of aluminum liquid and sublimate. The sublimation of SiC absorbs plasma heat, which will also decline the temperature of the plasma. As evidence, the surface temperature of 20vol% $SiC_p$/Al is higher than that of 50vol% $SiC_p$/Al composites.

## 5. Conclusions

This work built a new simulation model of single-pulsed arc discharge of $SiC_p$/Al matrix materials, the following conclusions can be drawn.

(1) The SiC-matrix cell geometric model for the heat conduction calculations of $SiC_p$/Al matrix materials is feasible. The model build in this work improves the simulation accuracy observably compared to the previous model.
(2) The highest surface temperature of $SiC_p$/Al workpiece is higher than 3300 K and the high temperature is found to concentrate on the surface layers of the workpiece, especially when the SiC fraction is high. Also, the peak value of the workpiece surface temperature decreases with the increase of SiC fraction.
(3) At the evaporation point of Al and SiC, the temperature fluctuation can be found respectively because of the high latent heat of Al and SiC. Compared to latent heat, the SiC particle-Al matrix interface resistance has less influence on temperature distribution.
(4) Two mechanisms in the temperature increasing process can be known, i.e., the evaporation of SiC and Al, and the melting of Al, the former occurs on the surface of the workpiece, the later exits in the material interior.
(5) Temperature increasing tendency is almost the same regardless of the SiC fractions, the melting and evaporation of different $SiC_p$/Al composites should be similar, and the difference lies in the ejection process of the melton material.

## Acknowledgments

This work was supported by the following foundations: Natural Science Foundation of China (Nos. 51975371, 51575351), Innovation and Entrepreneurship Project for High-level Talents in Jiangsu Province (No. 164040022), Youth science and Technology Innovation Foundation of NJFU of China (No. CX2018017).

## References

1. Ozben T, Kilickap E, Cakır O. Investigation of mechanical and machinability properties of SiC particle reinforced Al-MMC. *J Mater Process Tech* 2000;**198**(1–3):220–5.
2. Huang Y, Ouyang QB, Zhang D, et al. Carbon materials reinforced aluminum composites: a review. *Acta Metall Sin-engl* 2014;**27**(5):775–86.
3. Xiang DH, Shi ZL, Feng HR, et al. Finite element analysis of ultrasonic assisted milling of $SiC_p$/Al composites. *Int J Adv Manuf Tech* 2019;**105**(7–8):3477–88.
4. Zhou M, Wang M, Dong GJ. Experimental investigation on rotary ultrasonic face grinding of $SiC_p$/Al composites. *Mater Manuf Process* 2016;**31**(5):673–8.
5. Han JJ, Hao XQ, Li L, et al. Milling of high volume fraction $SiC_p$/Al composites using PCD tools with different structures of tool edges and grain sizes. *Int J Adv Manuf Tech* 2017;**92**(5–8):1875–82.
6. Kadivar MA, Akbari J, Yousefi R, et al. Investigating the effects of vibration method on ultrasonic-assisted drilling of Al/$SiC_p$ metal matrix composites. *Robot Cim-int Manuf* 2014;**30**(3):344–50.
7. Xiang JF, Xie LJ, Gao FN, et al. Diamond tools wear in drilling of $SiC_p$/Al matrix composites containing copper. *Ceram Int* 2018;**44**(5):5341–51.
8. Wang YF, Liao WH, Yang K, et al. Investigation on cutting mechanism of $SiC_p$/Al composites in precision turning. *Int J Adv Manuf Tech* 2019;**100**(1–4):963–72.
9. Aurich JC, Zimmermann M, Schindler S, et al. Turning of aluminum metal matrix composites: influence of the reinforcement and the cutting condition on the surface layer of the workpiece. *Adv Manuf* 2016;**4**(3):225–36.
10. Wang T, Xie LG, Wang XB, et al. PCD tool performance in high-speed milling of high volume fraction $SiC_p$/Al composites. *Int J Adv Manuf Tech* 2015;**78**(9–12):1445–53.
11. Huang ST, Guo L, He HT, et al. Experimental study on $SiC_p$/Al composites with different volume fractions in high-speed milling with PCD tools. *Int J Adv Manuf Tech* 2018;**97**(5–8):2731–9.
12. Xiang JF, Pang SQ, Xie LJ, et al. Mechanism-based FE simulation of tool wear in diamond drilling of $SiC_p$/Al composites. *Materials* 2018;**11**(2):E252.
13. Zheng W, Zhou M, Zhou L. Influence of process parameters on surface topography in ultrasonic vibration-assisted end grinding of $SiC_p$/Al composites. *Int J Adv Manuf Tech* 2017;**91**(5–8):2347–58.
14. Bhuyan RK, Routara BC. Optimization the machining parameters by using vikor and entropy weight method during EDM process of Al-18% $SiC_p$ metal matrix composite. *Decision Sci Lett* 2016;**5**(2):269–82.
15. Singh B, Kumar J, Kumar S. Investigation of the tool wear rate in tungsten powder-mixed electric discharge machining of AA6061/10% $SiC_p$ composite. *Mater Manuf Process* 2016;**31**(4):456–66.
16. Satpathy A, Tripathy S, Senapati NP, et al. Optimization of EDM process parameters for alsic-20% SiC reinforced metal matrix composite with multi response using topsis. *Mater Today: Proc* 2017;**4**(2):3043–52.
17. Tang L, Ren L, Zhu QL. Edm multi-pulse temperature field simulation of SiC/Al functionally graded materials. *Int J Adv Manuf Tech* 2018;**97**(5–8):2501–8.
18. Jarosz K, Nieslony P, Löschner P. Investigation of the effect of process parameters on surface roughness in EDM machining of ORVAR® supreme die steel. *Adv Manuf Eng Mater* 2019;333–40.
19. Meshcheriakov G, Nosulenko V, Meshcheriakov N, et al. Physical and technological control of arc dimensional machining. *CIRP Ann* 1988;**37**(1):209–12.
20. Chen XK, Zhou JP, Wang KD, et al. Experimental research on the influence of dielectrics on short electric arc machining of GH4169. *J Braz Soc Mech Sci* 2020;**42**(1):1–12.



Please cite this article in press as: CHEN J et al. Simulation of temperature distribution and discharge crater of $SiC_p$/Al composites in a single-pulsed arc discharge, *Chin J Aeronaut* (2020), https://doi.org/10.1016/j.cja.2020.05.033

21. Zhu G, Zhang QH, Wang HJ, et al. Machining behaviors of short electrical arc milling with high frequency and high voltage pulses. *Int J Adv Manuf Tech* 2017;**90**(1–4):1067–74.
22. Wang F, Liu YH, Tang ZM, et al. Ultra-high-speed combined machining of electrical discharge machining and arc machining. *P I Mech Eng B-J Eeg* 2014;**228**(5):663–72.
23. Wang F, Liu YH, Zhang YZ, et al. Compound machining of titanium alloy by super high speed EDM milling and arc machining. *J Mater Process Tech* 2014;**214**(3):531–8.
24. Zhang M, Zhang QH, Dou LY, et al. Effects of flushing on electrical discharge machining and electro-arc machining. *P I Mech Eng B-J Eng* 2016;**230**(2):293–302.
25. Zhao WS, Gu L, Xu H, et al. A novel high efficiency electrical erosion process-blasting erosion arc machining. *Procedia Cirp* 2013;**6**:621–5.
26. Chen JP, Gu L, Xu H, et al. Study on blasting erosion arc machining of Ti-6Al-4V alloy. *Int J Adv Manuf Tech* 2016;**85**(9–12):2819–29.
27. Xu H, Gu L, Chen JP, et al. Machining characteristics of nickel-based alloy with positive polarity blasting erosion arc machining. *Int J Adv Manuf Tech* 2015;**79**(5–8):937–47.
28. Gu L, Chen JP, Xu H, et al. Blasting erosion arc machining of 20 vol.% SiC/Al metal matrix composites. *Int J Adv Manuf Tech* 2016;**87**(9–12):2775–84.
29. Chen JP, Gu L, Zhu YM, et al. High efficiency blasting erosion arc machining of 50 vol.% SiC/Al matrix composites. *P I Mech Eng B-J Eng* 2018;**232**(12):2226–35.
30. Chen JP, Gu L, Liu X, et al. Combined machining of SiC/Al composites based on blasting erosion arc machining and CNC milling. *Int J Adv Manuf Tech* 2018;**96**(1–4):111–21.
31. Gu L, Chen JP, Zhu YM, et al. Influence of reinforcement particles on the mechanism of the blasting erosion arc machining of SiC/Al composites. *Int J Adv Manuf Tech* 2018;**99**(5–8):1119–29.
32. Kawai C. Effect of interfacial reaction on the thermal conductivity of Al-SiC composites with SiC dispersions. *J Am Ceram Soc* 2001;**84**(4):896–8.
33. Nan CW, Li XP, Birringer R. Inverse problem for composites with imperfect interface: determination of interfacial thermal resistance, thermal conductivity of constituents, and microstructural parameters. *J Am Ceram Soc* 2000;**83**(4):848–54.
34. Gu L, Zhu YM, He GJ, et al. Coupled numerical simulation of arc plasma channel evolution and discharge crater formation in arc discharge machining. *Int J Heat Mass Tran* 2019;**135**:674–84.
35. Wei R, Song S, Yang K, et al. Thermal conductivity of 4H-SiC single crystals. *J Appl Phys* 2013;**113**(5) 053503.
36. Gao YB, Zhou Y, Wu BX, et al. Time resolved experimental study of silicon carbide ablation by infrared nanosecond laser pulses. *J Manuf Sci E-T Asme* 2011;**133**(2) 021006.
37. Reitano R, Baeri P. Nanosecond laser-induced thermal evaporation of silicon carbide. *Int J Thermophys* 1996;**17**(5):1079–87.
38. Samant AN, Daniel C, Chand RH, et al. Computational approach to photonic drilling of silicon carbide. *Int J Adv Manuf Tech* 2009;**45**(7–8):704–13.
39. Duc DH, Naoki I, Kazuyoshi F. A study of near-infrared nanosecond laser ablation of silicon carbide. *Int J Heat Mass Tran* 2013;**65**:713–8.
40. Zhao YH, Kunieda M, Abe K. EDM mechanism of single crystal SiC with respect to thermal, mechanical and chemical aspects. *J Mater Process Tech* 2016;**236**:138–47.
41. Qian JM, Jin ZH, Wang XW. Porous SiC ceramics fabricated by reactive infiltration of gaseous silicon into charcoal. *Ceram Int* 2004;**30**(6):947–51.
42. Leitner M, Leitner T, Schmon A, et al. Thermophysical properties of liquid aluminum. *Metall Mater Trans A* 2017;**8**(6):3036–45.
43. Hasselman DP, Donaldson KY, Geiger AL. Effect of reinforcement particle size on the thermal conductivity of a particulate-silicon carbide reinforced aluminum matrix composite. *J Am Ceram Soc* 1992;**75**(11):3137–40.
44. Tao J, Ni J, Shih AJ. Modeling of the anode crater formation in electrical discharge machining. *J Manuf Sci E-T Asme* 2012;**134**(1) 011002.
45. Yeo SH, Kurnia W, Tan PC. Electro-thermal modelling of anode and cathode in micro-EDM. *J Phys D Appl Phys* 2007;**40**(8):2513.
46. Patel MR, Barrufet MA, Eubank PT, et al. Theoretical models of the electrical discharge machining process. ii. The anode erosion model. *J Appl Phys* 1989;**66**(9):4104–11.
47. Shahri HR, Mahdavinejad R, Ashjaee M, et al. A comparative investigation on temperature distribution in electric discharge machining process through analytical, numerical and experimental methods. *Int J Mach Tool Manu* 2017;**114**:35–53.
48. Yue XM, Yang XD, Tian J, et al. Thermal, mechanical and chemical material removal mechanism of carbon fiber reinforced polymers in electrical discharge machining. *Int J Mach Tool Manu* 2018;**133**:4–17.
49. Ming WY, Zhang Z, Wang SY, et al. Comparative study of energy efficiency and environmental impact in magnetic field assisted and conventional electrical discharge machining. *J Clean Prod* 2019;**214**:12–28.